ACS SENSORS

pubs.acs.org/acssensors

Article

Nanostructuring Synergetic Base-Stacking Effect: An Enhanced Versatile Sandwich Sensor Enables Ultrasensitive Detection of MicroRNAs in Blood

Xin-Xin Peng, Tongtong Guo, Hao Lu, Linlin Yue, You Li, Dan Jin, Guo-Jun Zhang,* and Fan Yang*

Cite This: *ACS Sens.* 2020, 5, 2514−2522

Read Online

ACCESS | Metrics & More | Article Recommendations | Supporting Information

ABSTRACT: MicroRNA (MiRNA)-based noninvasive diagnostics are hampered by the challenge in the quantification of circulating miRNAs using a general strategy. Here, we present a base-stacking effect-mediated ultrasensitive electrochemical miRNA sensor (BSee-miR) with a universal sandwich configuration. In the BSee-miR, a short DNA probe (10 nucleotides) self-assembled on a gold electrode surface could effectively capture the target miRNA synergizing with another sequence based on coaxial sandwich base-stacking, which rivals the fully complementary strength. Importantly, such a sandwich structure is flexible to incorporate signal amplification strategies (e.g., biotin−avidin) that are usually difficult to achieve in short sequence detection. Using this design, the BSee-miR achieves a broad dynamic range with a detection limit down to 7.5 fM. Furthermore, we found a high-curvature nanostructuring synergetic base-stacking effect that could improve the sensitivity of the BSee-miR by two orders of magnitude (79.3 aM). Our BSee-miR also has a single-base resolution to discriminate the highly homologous miRNAs. More importantly, this approach is universal and has been used to probe target miRNAs varying in sequences and secondary structures. Our ultrasensitive sensor could detect miRNA in cell lysates and human blood and distinguish cancer patients from normal individuals, promising a versatile tool to measure clinically relevant miRNAs for tumor diagnostics.

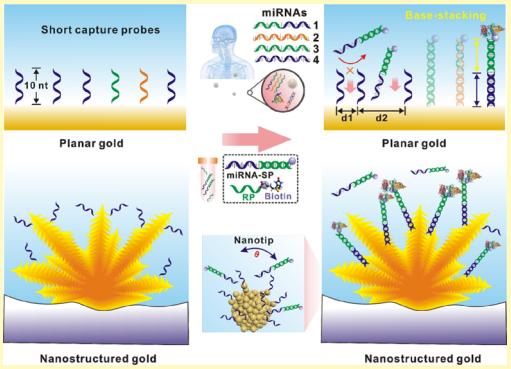

KEYWORDS: *circulating miRNAs, gold nanostructures, electrochemistry, base-stacking effect, biosensor*

MicroRNAs (miRNAs) are a class of evolutionarily conserved non-coding small RNAs that regulate various pathophysiological processes in humans.[1] Increasing evidence shows that circulating miRNAs in blood highly correlate with cancer metastatic progression and are emerging as important tumor biomarkers.[2] However, accurate miRNA quantitation in biofluids remains a challenge because of their small size (18−24 nucleotides, nt), low abundance, and high homology.[3,4] Despite the gold standard approaches, such as quantitative reverse transcription-polymerase chain reaction (qRT-PCR) and sequencing, many sensitive biosensing strategies have also been proposed to enable miRNA detection.[5−12] Nevertheless, these methods either require cDNA synthesis, exonuclease, sophisticated probe design, or ultrasensitive transducers.[13−15] Surface-based sandwich strategies feature high sensitivity and specificity compatible with different signal amplification means,[16] whereas the direct sandwich detection for small-sized miRNAs remains a hurdle.[6,9] Although locked nucleic acid (LNA) and peptide nucleic acid (PNA) probes could improve the capture of target miRNA in sandwich assays,[17,18] the costly and stringent probe synthesis limits their broad application in miRNA profiling. Base-stacking effects have been proved to boost the hybridization between short strands, such as miRNAs.[19,20] However, the selection of DNA capture probes (CPs) in direct miRNA sandwich assay is empirical and remains elusive. All of these inspire us to design an affordable universal approach adapted to most, if not all, miRNA detection.

Here, we demonstrate a nanostructuring-enhanced, base-stacking effect-mediated electrochemical miRNA sensor (Bsee-miR) with a universal sandwich construct. By exploiting a rational DNA probe partially complementary to target miRNA, the Bsee-miR has a stable sandwich configuration via a coaxial base-stacking effect, which contributes to additional stability in nucleic acid hybridization.[19,20] Using this strategy, the Bsee-miR is capable of probing multiple miRNAs (miR21, miR10b, miR223, and miR141) at an ultrasensitive level regardless of their sequences and secondary structures. Through engineering

Received: April 15, 2020
Accepted: July 15, 2020
Published: July 15, 2020

a high-curvature nanostructuring interface, we found an enhanced signal response probably due to the enlarged deflection angles that permit the access of target molecules with attenuated steric hindrance.[21−26] Such an enhanced Bsee-miR achieves a higher sensitivity and wider dynamic range that largely overlaps with the range of miRNA concentrations (~600−2900 pg/mL, equivalent to ~80−400 pM) naturally existing in cancer patient blood.[2,27] Meanwhile, the double check by sandwich mode is able to ensure high specificity. Using the high-performance Bsee-miR, we can well distinguish cancer patients from healthy individuals. These advantages make the universal Bsee-miR promising in precision medicine.

EXPERIMENTAL SECTION

Materials and Chemicals. Gold chloride trihydrate ($HAuCl_4 \cdot 3H_2O$, ≥99.9%) was purchased from Aladdin (Shanghai, China), poly(ethyleneimine) (PEI), poly(acrylic acid) (PAA), tris(2-carboxyethyl)phosphine hydrochloride (TCEP), 6-mercapto-1-hexanol (MCH), and RNaseZAP solution were provided by Sigma-Aldrich (St. Louis, MO, U.S.A.). Bovine serum albumin (BSA) was obtained from Wuhan Servicebio Technology (Wuhan, China). Tetramethylbenzidine (TMB) substrate (Enhanced K-blue substrate, H_2O_2 included) was purchased from Neogen (Lansing, USA). Horseradish peroxidase (HRP)-conjugated streptavidin (SA-HRP) was obtained from Invitrogen (California). All chemicals were of analytical reagent grade. Ultrapure water (18.2 MΩ, Millipore Corp.) was used in the whole assay. All DNA oligonucleotides were purchased from Sangon Inc (Shanghai, China). All miRNAs were synthesized and purified by Takara Biotechnology (Dalian, China). All sequences of the above oligonucleotides are listed in Table S1. Breast cancer, liver cancer, non-small cell lung cancer (NSCLC), and healthy human blood samples were supplied by the Central Hospital of Wuhan (Wuhan, China), which was approved by the Ethics Committee of the Central Hospital of Wuhan.

Apparatus and Measurements. All electrochemical measurements were carried out by a CHI 660D electrochemical workstation (CH Instruments Inc., Austin, TX). A conventional three-electrode configuration was implemented, containing a gold working electrode, a platinum wire auxiliary electrode, and a Ag/AgCl reference electrode. Screen-printed carbon electrodes (SPCEs, provided by Shanghai Institute of Applied Physics) are composed of a 3 mm diameter carbon working electrode, a silver pseudo-reference electrode, a carbon counter-electrode, and a customized USB converter. Chronoamperometry was employed to grow gold nanostructures (AuNSs) on the SPCE surface. The AuNS morphologies were characterized by scanning electron microscopy (SEM, Zeiss Merlin Compact). Square-wave voltammetry (SWV) was used by scanning the potential from −0.4 to −0.1 V in 10 mM PBS buffer (50 mM NaCl and 10 mM $MgCl_2$, pH 7.4) with a step potential: 1 mV, frequency: 60 Hz, and amplitude: 50 mV. The amperometric $i-t$ curve was obtained and cyclic voltammetry (CV) were performed in TMB solution with a potential of +0.15 V for the gold electrode and −0.2 V for the SPCE, respectively.

Fabrication of BSee-miR Sensor. Au electrodes (2 mm diameter, CH Instruments Inc.) were first cleaned as per the previous protocols.[28,29] After cleaning and drying, the electrodes were immediately incubated with 5.5 μL of TCEP-treated HS-DNA varying in concentrations or lengths for overnight self-assembly as CPs. The modified electrodes were subsequently blocked by 2 mM MCH and were further exposed to the mixture of target miRNA and biotinylated stacking probe (SP) for 1 h. Next, 5.5 μL of SA-HRP was dropped onto the modified electrodes for 30 min. Prior to amperometric detection in TMB solution, the electrodes were thoroughly rinsed with 1× PBST (0.1% Tween) to minimize the nonspecific adsorption of SA-HRP on the gold surface. The SPCE-based BSee-miR sensor was fabricated based on a previous protocol.[22] Briefly, polyelectrolyte multilayer (three bilayers of PEI/PAA) was first alternately self-assembled on the SPCE surface to modulate the morphology of AuNSs during electrochemical deposition. In the presence of 3 mg/mL $HAuCl_4$ (NaCl), a potential with −0.1 V was used to grow AuNSs within 1200 s. Subsequently, 20 μL CPs treated by TCEP were dropped on AuNSs−SPCE for overnight immobilization. After blocking with 2 mM MCH for 1 h, the AuNSs−SPCEs were incubated in 20 μL of the mixture of target miRNA and biotin−SP for 1 h. After further blocking by 1% BSA, 20 μL of SA-HRP was dropped on the SPCEs and thoroughly rinsed with 1× PBST followed by amperometric detection in TMB with H_2O_2.

Cell Culture and RNA Isolation. Different human cancer cell lines (e.g., lung cancer A549, breast cancer MCF-7, cervical cancer HeLa, hepatocellular cancer (HepG-2), and normal human hepatocyte cells (HL7702) were cultured in fresh Dulbecco's modified essential medium (DMEM, Cellgro) containing 10% fetal bovine serum, 1% penicillin (100 U/mL), and streptomycin (100 μg/mL). All cells were kept in a humidified atmosphere with 5% CO_2 at 37 °C. Total RNA samples from the different cell lines (varying in concentrations) and human blood were extracted by the miRNA isolation Kit (Tiangen Biotech) according to the recommended instructions of the manufacturer.

RESULTS AND DISCUSSION

Design of Nanostructuring Synergetic Bsee-miR Sensor. We designed a nanostructuring-enhanced Bsee-miR sensor that complements a base-stacking effect with a target miRNA-bridged sandwich construct to enable detection of circulating miRNAs with high specificity and sensitivity (Figure 1). Short DNA recognition sequences (10 nt) can use Au−S

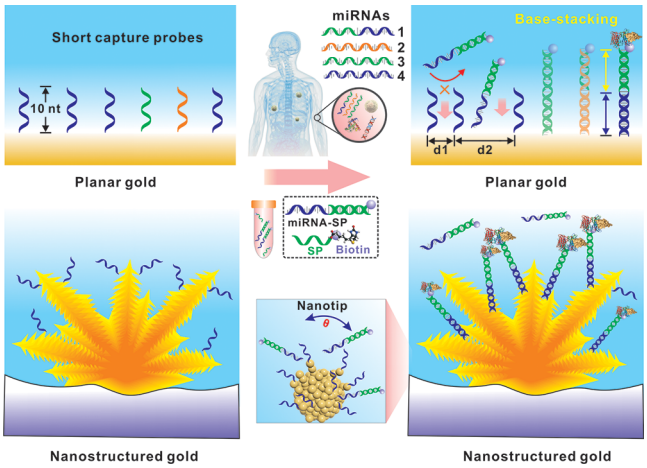

Figure 1. Schematic of nanostructuring synergetic Bsee-miR sensor. Short DNA CP cooperates with SP in the prehybridized duplex (miRNA-SP) complementing target miRNA to form a sandwich structure via base-stacking effect, making Bsee-miR a versatile scheme adapted to detect different miRNAs. Using the large deflection angle (θ) of high-curvature gold nanostructures (nanotip) to boost hybridization between CP and miRNA-SP duplex through reduced steric hindrance that usually exists in surface-based molecular recognition (lateral distance, d1 and d2), an enhanced Bsee-miR is compatible with available sandwich signal amplification strategies, such as biotin−avidin−HRP catalysis system, allowing for quantification of target miRNAs.

bonds to self-assemble on a planar gold surface as CPs. Considering such a short length is not strong enough to capture the complementary miRNA, we implemented base-stacking effect to synergize the short CP and SP together serving as a complementary probe to enhance the binding of target miRNAs without resorting to the costly PNA or LNA probes, which are usually used in miRNA detection.[17,18] This

https://dx.doi.org/10.1021/acssensors.0c00772
ACS Sens. 2020, 5, 2514−2522

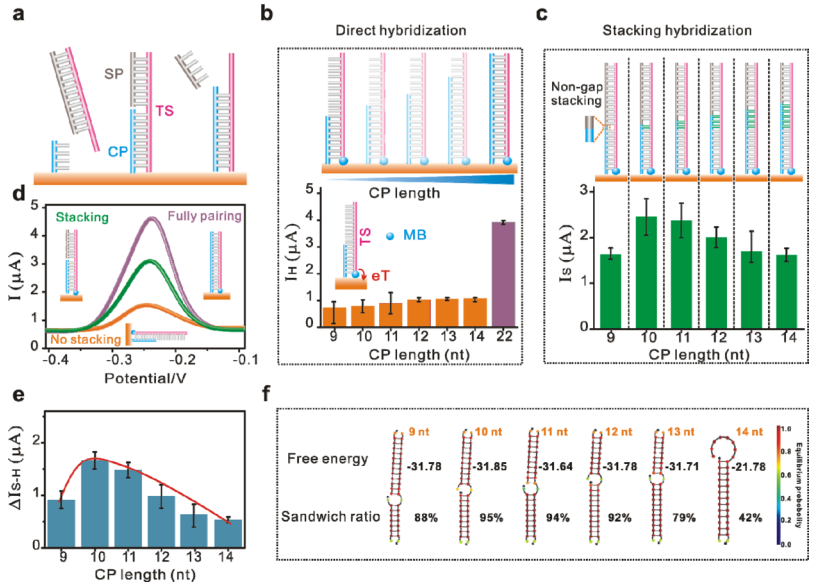

Figure 2. Rational selection of CPs for Bsee-miR. (a) Schematic of surface-confined hybridization between CPs varying in length and prehybridized DNA21-SP. (b) Schematic and electrochemical response for direct hybridization between CPs with different lengths (from 9 to 14 and 22 nt) and DNA21-MB. (c) Schematic and electrochemical response for base-stacking hybridization among CPs varying in lengths (from 9 to 14 nt), corresponding SPs (from 13 to 8 nt), and DNA21-MB. (d) SWV signals of 10 nt CP-based direct (no stacking) and stacking hybridization with DNA21-MB, and the 22 nt full complementarity. (e) Signal changes (ΔI_{S-H}) between the sandwich structure (I_S) and the direct CP−TS hybridization (I_H) induced by different CPs. (f) CP-DNA21-SP hybridization simulated by NUPACK analysis. Error bars represent the standard deviations of measurements (n = 3).

short CP-based sandwich configuration provides a versatile strategy to probe various miRNAs regardless of their secondary structures and sequences. With the prehybridization between target miRNA and SP, the surface-confined CPs can specifically hybridize with the exposed complementary domain in the partial duplex (miRNA-SP) via coaxial base-stacking effect,[6,19,20] where two or more single-stranded nucleic acids hybridize with the longer single-stranded nucleic acid in a contiguous tandem manner with non-gap arrangement. The base-stacking at the junction of the adjacent short-stranded nucleic acids (e.g., CP and SP) brings additional stability and efficiency.[30] This property renders them stable hybridization with miRNA targets, approaching that with fully complementary CPs.[19]

To improve such effects, we engineered a high-curvature gold nanostructuring interface (Figure 1), which can enlarge the deflection angle (θ) of CPs on the sensor surface to facilitate the access of targets and accelerate the interfacial molecular collision through boosted mass diffusion.[22,23] Although the prehybridization of miRNA with SP is able to improve target capturing efficiency, especially at an ultralow level, both the high negative charge and large size of the miRNA-CP duplex would largely limit the molecular recognition on a negatively charged surface. Of note, this side-effect would be attenuated by hierarchical nanostructuring, which reduces steric hindrance and accelerates molecular diffusion contributing to the formation of the sandwich construct, compatible with many available signal amplification strategies.[16] In Bsee-miR, small redox molecules (TMB) serve as signaling mediators catalyzed by HRP that binds to SP through avidin−biotin conjugation. The catalytic current in the i−t curve can reflect the amounts of target miRNAs.[10] Therefore, using this approach, we can quantify a variety of target miRNAs through the synergy between base-stacking effect-mediated sandwich hybridization and nanostructuring-enhanced detection performance.

Rational Selection of CPs. As shown in Figure 2a, hybridization efficiency among the CP, short target sequence (TS), and SP depends heavily on the length of the CP and SP, whereas in the Bsee-miR, their lengths are governed by TS (i.e., miRNA). When CP is too long, the SP becomes very short, which would disassociate SP from the TS and thus degrade the intended sandwich configuration even with a coaxial stacking effect, and vice versa. As the length of CP increases, the CP−TS hybridization strength rises, gradually approaching the fully complementary pairing (Figure 2b). However, such a direct partial hybridization would mask the advantages of sandwich assays in sensitivity and specificity, which usually demand exonuclease or ultrasensitive transducers to enable sensitive miRNA analysis.[7,14,22,31] To explore the rational length of CP in Bsee-miR, we designed multiple CPs varying in lengths concomitant with different SPs targeting the DNA21 (DNA sequence of miR21, 22 nt). Without SP, all CPs can effectively hybridize with DNA21-MB (methylene blue) for electrochemical signaling. We found a gradual increment of current signal with the increasing length of CPs (from 9 to 14 nt), whereas the signal intensity by the 14 nt CP is less than 50% of that by fully pairing, suggesting a relatively low hybridization efficiency (Figure 2b). In the presence of SP, we observed a para-curve-like signal response trend and the highest signal occurred for CPs at 10 nt (Figure 2c), indicating a potential hybridization synergy varying in CPs and SPs. The SWV signal by 10 nt CP (12 nt SP) is relatively close (~70%) to that induced by fully complementary hybridization but much higher than that without SP (by 2 folds) (Figure 2d). These results signify a favorable base-stacking effect offered by 10 nt DNA CPs cooperating with a 12 nt SP in miR21 detection.

https://dx.doi.org/10.1021/acssensors.0c00772
ACS Sens. 2020, 5, 2514−2522

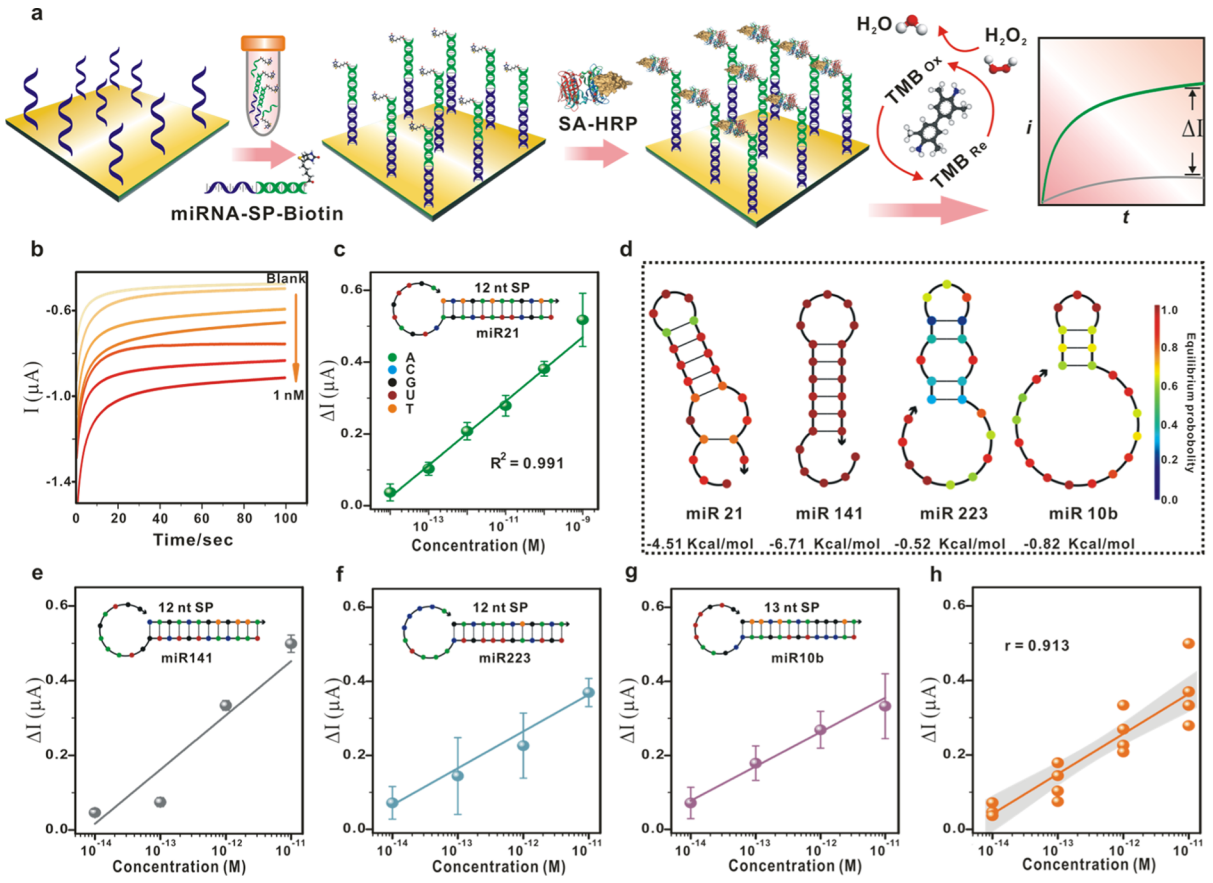

Figure 3. Sensitivity and generality of Bsee-miR sensor. (a) Schematic of Bsee-miR sensor with an optimal sandwich configuration coupling HRP to catalyze redox TMB system for signal-amplified miRNA detection. (b) Amperometric i−t curves of Bsee-miR in response to target miR21 with different concentrations ranging from 10 fM to 1 nM. (c) Linear relationship between the signal change (ΔI) and the logarithm of target miR21 concentrations. (d) Secondary structure analysis of four distinct sequences (miR21, miR141, miR223, and miR10b) by NUPACK. (e−g) Bsee-miR enables the detection of different miRNAs, such as miR141 (e), miR223 (f), and miR10b (g), displaying the signal change (ΔI) vs different target concentrations from 10 fM to 10 pM. (h) Correlation of signal variations induced by the four miRNA sequences at the same concentrations measured by Bsee-miR. Error bars represent the standard deviations of measurements (n = 3).

We also found the 10 nt CP resulting in the largest signal change ΔI_{S-H}, defined as the signal variation between sandwich structure (I_S) and the direct CP−TS hybridization (I_H) (Figures 2e and S1), suggesting the maximal base-stacking effect templated by DNA21. It is reported that if the adjacent stacking sequences (e.g., CP and SP) are T_m equalized, they will maximize the benefits of base-stacking effect.[19,20] We thus calculated the T_m of different CPs and the corresponding SPs in hybridization to TS, observing that the T_m of CP at 10 and 11 nt is in close proximity to the corresponding SP at 12 and 11 nt, respectively (Table S2). These results agree well with the current signals induced by sandwich constructs based on the stacking effect (Figure 2c). Besides that, the secondary structure of DNA probes also affects their hybridization efficiency. Next, we analyzed the free energy of SP-DNA21 and CP-DNA21 duplex to evaluate the stability of their secondary structures (Table S3). Figure 2f shows the lowest free energy (−31.85 kcal/mol) and the highest ratio (95%) of the sandwich construct assembled by 10 nt CP (12 nt SP and DNA21) at room temperature. We attribute these advantages to the synergy between coaxial base-stacking effect and favorable secondary structures of DNA probes. Of note, the findings of Figure 2c were not sequence-specific, which could be extended to different miRNA detection.[32]

Sensitive and General Bsee-miR Sensor. Based on the optimal sandwich configuration, we designed a Bsee-miR sensor to enable sensitive miRNA detection by coupling HRP to catalyze a redox TMB system for signal amplification (Figure 3a). By taking miR21 as a target, we first verified the processes of probe self-assembly, miR21 hybridization, and biotin−avidin binding on the gold electrode surface using electrochemistry. CV and electrochemical impedance spectroscopy were employed to confirm the stepwise construction of the sensing interface in the presence of the redox pair of $[Fe(CN)_6]^{3-/4-}$ (Figure S2). Next, we measured the target miR21-induced signal using the 10 nt CP-mediated sandwich assay and found a clear current signal by the amperometric i−t curve (Figure S3), suggesting a feasible miRNA sensing with the Bsee-miR. Given the steric hindrance that governs the surface-based molecular recognition, we next explored the CP density on electrode surface to maximize the hybridization efficiency between CP and SP-miR21 duplex (Figure S4). By assembling 10 nt CPs on gold electrode with concentrations spanning from 0.5 to 2 μM, we observed the largest signal change ΔI occurred at 0.5 μM (10 nM miR21) equal to 3.1 nm intermolecular gap.[29,33,34] This distance is able to render the assembled short CP upright and accessible to SP-miR21 duplex with a larger size.

https://dx.doi.org/10.1021/acssensors.0c00772
ACS Sens. 2020, 5, 2514−2522

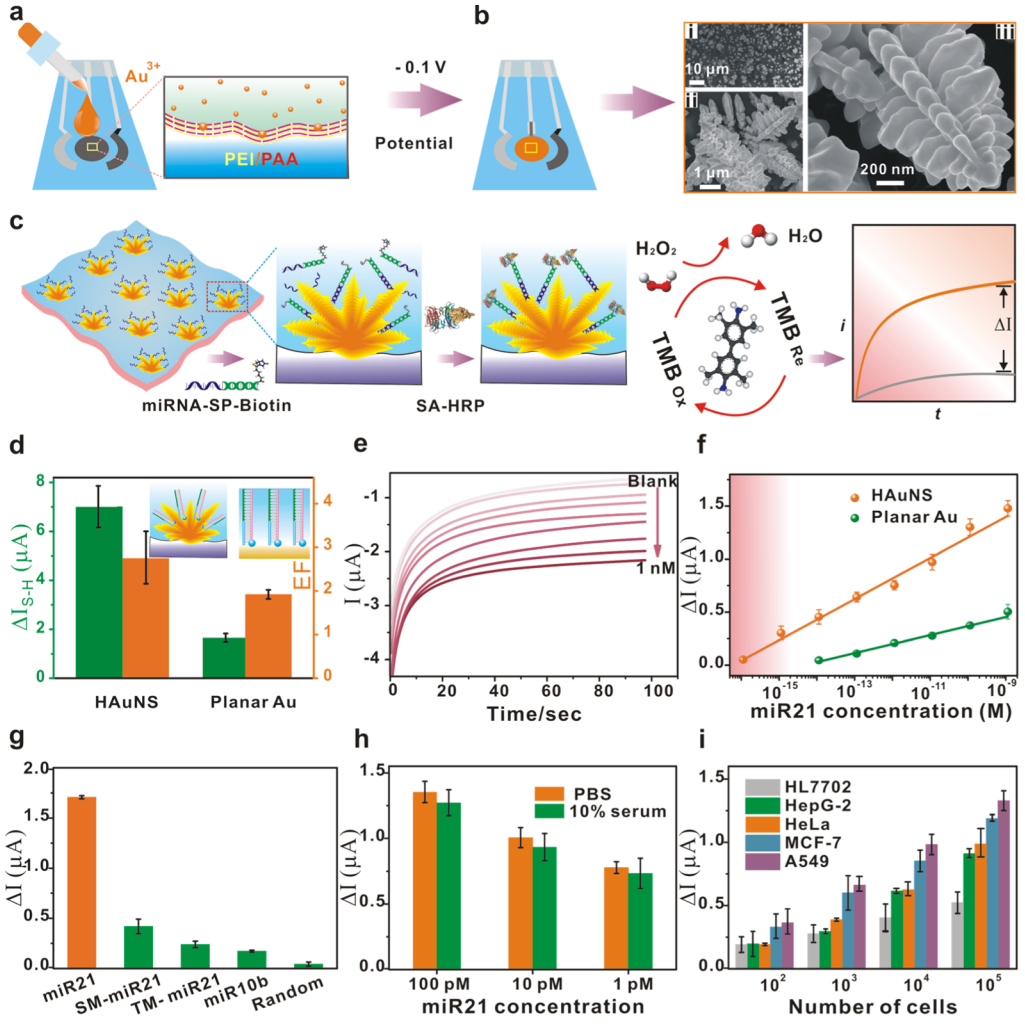

Figure 4. Nanostructuring-enhanced Bsee-miR. (a) Schematic of polyelectrolyte multilayer-assisted electrodeposition of gold nanostructures. (b) Large area of SEM image of HAuNS array decorated on SPCE (i), individual HAuNSs SEM image (ii), and the zoom-in nanobranching structure (iii). (c) Schematic of nanostructuring-enhanced Bsee-miR sensor with an optimal sandwich configuration coupling HRP to catalyze redox TMB system for miRNA detection. (d) Comparison between Bsee-miR with and without nanostructuring in response to DNA21-MB. EF = $\Delta I_{S-H}/I_H$. (e) Amperometric $i-t$ curves of nanostructuring-enhanced Bsee-miR in response to target miR21 varying in concentrations from 100 aM to 1 nM. (f) Logarithmic plot of the signal change (ΔI) vs target miR21 concentrations, and the comparison of dynamic range between Bsee-miR with and without nanostructuring. (g) Selectivity of nanostructuring-enhanced Bsee-miR. (h) Comparison of signal change for enhanced Bsee-miR in response to miR21 (100, 10, 1 pM) in PBS and 10% human serum. (i) Enhanced Bsee-miR allows to detect the target miR21 in total RNA extracted from A549, MCF-7, HeLa, HepG-2, and HL7702 with different cell numbers (10^2, 10^3, 10^4, and 10^5 cells), respectively. Error bars represent the standard deviations of measurements (n = 3).

Based on the optimal parameters, we next utilized the Bsee-miR sensor to detect target miR21 with concentrations ranging from 10 fM to 1 nM. Figure 3b shows a typical concentration-dependent electrochemical response spanning 5 orders of magnitude. The current signal change (ΔI) was logarithmically related to the concentration of target miR21 across a wide dynamic range (Figure 3c). We achieved a linear regression equation expressed as ΔI = 0.09 lgC + 1.3, with a correlation coefficient (R^2 = 0.991), and a detection limit down to 7.5 fM estimated by $3\sigma/S$ (σ is the standard deviation of the blank signal and S is the slope of the fit line in Figure 3c). Such a high sensitivity is comparable or even superior to those miRNA sensors relying on exonuclease or ultrasensitive transducers (Table S4). The excellent performance of the Bsee-miR sensor probably profits from (i) the base-stacking effect that enhances the stability of hybridization and (ii) universal sandwich configuration-mediated signal amplification.[16]

We further explored the generality of our Bsee-miR sensor in detection of different miRNAs varying in secondary structures, sequences, and lengths. The most, if not all, miRNAs harbor self-complementary domains that would affect their CP design and hybridization events. For example, it is difficult to synthesize the fully complementary PNA probe for miR21 due to its intrinsic self-pairing. Figure 3d shows the secondary structure and free energy of four different types of miRNAs (miR21, miR223, miR141, and miR10b) at 25 °C, where each displays a stem-loop structure. Both miR21 and miR141 exhibit a relatively stable secondary structure, whereas miR223 and miR10b show weak configurations. Although these miRNAs are different in structures, sequences, and lengths, we found that the 10 nt CP was strong enough to capture the corresponding miRNAs on the basis of SP-mediated base-

https://dx.doi.org/10.1021/acssensors.0c00772
ACS Sens. 2020, 5, 2514−2522

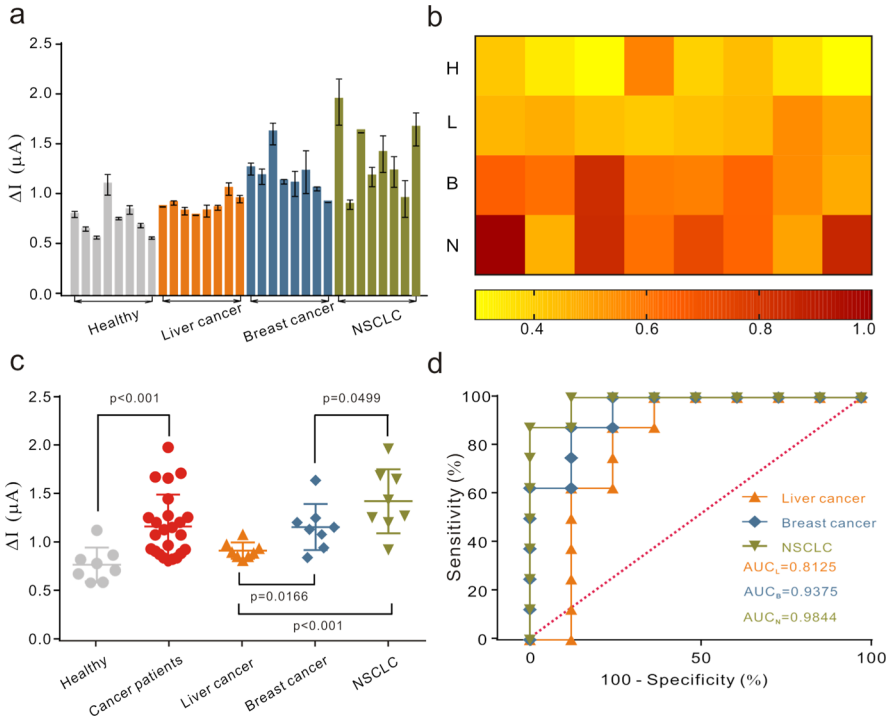

Figure 5. Nanostructuring-enhanced Bsee-miR enables to detect the target miR21 from clinical blood samples. (a) Signal change of enhanced Bsee-miR in response to miR21 from human plasma samples, including patients with liver cancer (n = 8), breast cancer (n = 8), NSCLC (n = 8), and 8 healthy volunteers. (b) Heat map illustrating the miR21 expression level across 24 different cancer patients (L: liver cancer, B: breast cancer, and N: NSCLC patients) and 8 healthy ones (H). (c) Significant expression difference of miR21 among patients with distinct cancer and the healthy donors. (d) ROC curve of enhanced Bsee-miR in response to miR21 in patients with diverse cancers. Error bars represent the standard deviations of measurements (n = 3).

stacking effect (Figure 3d–g). All structure simulations showed the linear domains in the miRNA-SP duplex for CP pairing (Figure 3d–g Inset). Using Bsee-miR sensor, we measured the current signal changes in response to each of them and observed a concentration-dependent increment with target concentration ranging from 10 fM to 10 pM (Figure 3e–g). This means that we can detect each of them at low concentrations, down to femtomolar levels. These results are consistent with that of miR21 showing the similar change trend and amplitude with a high correlation (r = 0.913, Figure 3h), suggesting that our sensor is universal to be exploited in miRNA profiling.[32]

Engineering a Nanostructuring-Enhanced Bsee-miR Sensor. Increasing number of studies reveal that nanostructures can boost interfacial molecular recognition through accelerated molecular diffusion and reduced steric hindrance.[23,24] These properties inspire us to explore whether the nanostructured interface could enhance the base-stacking effect in nucleic acid hybridization. We first engineered a high-curvature nanostructuring interface on SPCEs templated with their intrinsic nanoporous structure and polyelectrolyte multilayer coating (Figure 4a).[22,35] Using a single-step electrodeposition, we fabricated an array of hierarchical gold nanostructures (HAuNSs) in the presence of $HAuCl_4$ (3 mg/mL) with deposition potential (−0.1 V) for 20 min(Figure 4b). Each HAuNS represents an independent microelectrode that can protrude out of the SPCE surface permitting a solution-phase-like hybridization setting. Figure 4b used a zoom-in SEM image to show the typical hierarchical morphology of single HAuNSs. These high-curvature nanoarming branches can increase the deflection angle of molecular probes, making them more easily accessible by target molecules, particularly for the large molecular assemblies (e.g., prehybridized duplex) to enable sensitive miRNA detection (Figure 4c).

We next interrogated the base-stacking effect on this high-curvature nanostructuring interface. First, we employed CV to characterize the stepwise molecular assembly and electron transfer at the HAuNSs interface in the redox pair of $[Fe(CN)_6]^{3-/4-}$ (Figure S5). By assembling the 10 nt CP on HAuNSs with identical assembly concentration (0.5 μM) to that on atomically smooth gold surface, we observed a significant enhancement (~7 folds) in current signal change ($\Delta I_{S\text{-}H}$), in the presence of the same DNA21-MB (1 μM) and 12 nt SP (2 μM) (Figures 4d and S6), suggesting a synergetic coaxial base-stacking effect with high-curvature nanostructuring. The result was further confirmed by an enhancing factor (EF) ratio (EF ratio = EF_H/EF_P; $EF_H = \Delta I_{S-H}/I_H$ with HAuNS; $EF_P = \Delta I_{S-H}/I_H$ with planar Au). The EF ratio was calculated to be 1.42, signifying an enhancement of ~42% in signal response for each sandwich construct on HAuNS over on the planar Au surface.

We further explored the sensitivity of the enhanced Bsee-miR sensor. By measuring target miR21 with concentrations spanning from 100 aM to 1 nM, we observed a typical concentration-dependent i–t curve (Figure 4e). Figure 4f shows that the signal change (ΔI) is logarithmically related to miR21 concentration across 7 orders of magnitude with a linear regression equation (ΔI = 0.20 lgC + 3.29, R^2 = 0.990). Using an enhanced Bsee-miR, we achieved a sensitivity down to 79.3 aM, exceeding that without a nanostructuring interface by 2 orders of magnitude (Figure 4f). The result suggests that

https://dx.doi.org/10.1021/acssensors.0c00772
ACS Sens. 2020, 5, 2514–2522

nanostructuring can significantly improve the detection sensitivity of the Bsee-miR sensor. This attomolar sensitivity can rival those enzyme-based miRNA approaches, and even surpass that obtained on ultrasensitive sensors.[36] We reason such a high sensitivity arises primarily from the enhanced base-stacking effect and faster binding kinetics on the high-curvature nanostructuring interface.[19,22,24]

Next, we implemented the enhanced Bsee-miR to distinguish different miRNAs, including the perfectly matched (miR21), single-, two-base mismatched (SM and TM), miR10b, and random miRNA sequences. As shown in Figure 4g, the signal change by SM miRNA is less than 25% of that by fully complementary miR21 (lowered by 10-fold in concentration), and less than15% for the TM sequence, and a negligible variation for miR10b and random sequence. Such superior selectivity is probably ascribed to (i) the short DNA probe (10 nt CP)-mediated sandwich construct and (ii) nanostructuring-enhanced base-stacking effect. In this case, even a single-base mismatch would disassociate the weak duplex. Of note, this strategy has a single-base resolution against miRNAs at room temperature without the need of stringent thermal controlling, which is appropriate for on-site application.

We further examined the anti-interference of the enhanced Bsee-miR in complex biological samples. By spiking miR21 with different concentrations (from 1 to 100 pM) into the diluted human serum that might degrade the sensor performance due to multicomponents, we observed negligible signal variations between buffered saline (10 mM PBS) and 10% human serum (Figure 4h). We reason that the favorable anti-interference probably arises from the nanostructuring-enhanced specific hybridization via the base-stacking effect.

We next used Bsee-miR to explore the different expression levels of miR21 across five cell lines. Figure 4i displays the detected profiles of target miR21 in total RNA extracted from distinct cancer cells (e.g., A549, MCF-7, HeLa, and HepG-2 cells) and human normal liver cells (HL7702). We observed that the signal change gradually rise with the increment of lysated cells numbers from 10^2 to 10^5 (Figures 4i and S7).

We also found that the higher signal variation occurred by A549 and MCF-7 cells relative to others. As noticed, larger the number in lysated cells, higher is the signal difference between cancer and normal cells. The result suggests an over-expression of miR21 in A549 and MCF-7 cells relative to that in HepG-2 and HeLa cells (Figure S8), and particularly much higher than that in normal cells, which is consistent with the previous reports.[37,38] These performances allow the enhanced Bsee-miR to sensitively profile cancer miRNAs and selectively discriminate tumor cells for cancer diagnosis and treatment monitoring.

Clinical Assay with Nanostructuring-Enhanced Bsee-miR. To verify the practicability of Bsee-miR in clinical settings, we exploited the performance-enhanced sensor to detect circulating miR21 in human blood plasma. By collecting 32 human peripheral blood samples from a local hospital, including patients with liver cancer, breast cancer, NSCLC, and normal individuals (each of them in equal numbers, n = 8), we extracted total RNA from the clinical plasma specimens and analyzed them using a nanostructuring-enhanced Bsee-miR. We found that miR21 levels in cancer patients are higher than in healthy individuals, particularly for NSCLC and breast cancer patients with elevated expression level of miR21 (Figure 5a). As demonstrated in Figure 5b, the relative expression levels of miR21 were summarized and normalized as a heat map, which clearly shows the high expression of miR21 in patients with breast cancer and NSCLC, signifying the well-defined differentiation between them and the healthy donors by miR21. Using the t-test, we observed a significant difference in signal changes between healthy volunteers and cancer patients ($p < 0.001$) (Figure 5c). There is also a similar significant difference of miR21-responsive signal change among patients with distinct cancers, particularly between NSCLC and liver cancer patients ($p < 0.001$) (Figure 5c). Furthermore, the ROC (receiver operating characteristic) curve shows the highest accuracy (AUC = 0.9844) of circulating miR21 level in discrimination of NSCLC patients from healthy controls (Figure 5d). These results agree well with previous studies, which reveal the elevated expression level of miR21 in cancer patients.[39] The upregulation of miR21 usually occurs in NSCLC and breast cancer patients, probably arising from the activation of EGFR (epidermal growth factor receptor) signaling and receptor tyrosine kinase, respectively, with enhanced miR21 expression, which can predict clinical pathological features and poor prognosis.[40,41] Bsee-miR-based clinical assays evidence the potential of circulating miR21 as a biomarker in cancer diagnosis albeit limited by the small cohort. Of note, our nanostructuring-enhanced Bsee-miR provides an amplification-free, isothermal, and miniaturized platform toward clinical miRNA profiling, particularly in comparison to the current gold standard qRT-PCR.

CONCLUSIONS

In summary, we present a generalized Bsee-miR sensor harnessing nanostructuring synergetic coaxial stacking effect to enable circulating miRNA detection with single-base resolution and attomolar sensitivity. Using this strategy, we unify the advantages between nanostructuring-enhanced base-stacking effect and sandwich construct-induced signal amplification for ultrasensitive bioassay. Besides that, such a high-performance miRNA sensor has some additional features: (i) Based on base-stacking effect, a 10 nt DNA CP is strong enough to capture the target miRNA (~22 nt), without the need of costly PNA or LNA probes; (ii) high-curvature nanostructuring can synergize with base-stacking effect for developing a sensitive Bsee-miR sensor; (iii) target-bridged sandwich configuration is compatible with many signal-amplified strategies for ultrasensitive detection; and (iv) the double check between the CP and reporter probe guarantees the specificity in short miRNA detection. This design also represents a versatile strategy for miRNA profiling at room temperature regardless of their natural secondary structures and lengths. We anticipate that our Bsee-miR sensor can further complement functional nanostructures and/or external field-accelerated binding to enable rapid and universal detection of various clinically relevant nucleic acids (varying in lengths and secondary structures) for precision theranostics.[42−47]

ASSOCIATED CONTENT

Supporting Information

The Supporting Information is available free of charge at https://pubs.acs.org/doi/10.1021/acssensors.0c00772.

Involved oligonucleotides and corresponding sequences; feasibility of Bsee-miR sensor in HRP-TMB amplification system; difference of nanostructuring-enhanced

https://dx.doi.org/10.1021/acssensors.0c00772
ACS Sens. 2020, 5, 2514−2522

Bsee-miR sensor in detection of total RNA; T_m and free energy of hybridization; comparison of sensor performance; and SWV, CV, ESI, and miRNA detection from cells (PDF)

AUTHOR INFORMATION

Corresponding Authors

Guo-Jun Zhang − *School of Laboratory Medicine, Hubei University of Chinese Medicine, Wuhan 430065, China;* orcid.org/0000-0001-9096-9226; Email: zhanggj@hbtcm.edu.cn

Fan Yang − *School of Pharmacy, Guangxi Medical University, Nanning 530021, China;* orcid.org/0000-0002-8490-4183; Email: yangfan@gxmu.edu.cn

Authors

Xin-Xin Peng − *School of Laboratory Medicine, Hubei University of Chinese Medicine, Wuhan 430065, China*

Tongtong Guo − *School of Pharmacy, Guangxi Medical University, Nanning 530021, China*

Hao Lu − *School of Laboratory Medicine, Hubei University of Chinese Medicine, Wuhan 430065, China*

Linlin Yue − *School of Laboratory Medicine, Hubei University of Chinese Medicine, Wuhan 430065, China*

You Li − *School of Laboratory Medicine, Hubei University of Chinese Medicine, Wuhan 430065, China; Department of Medical Laboratory, the Central Hospital of Wuhan, Tongji Medical College, Huazhong University of Science and Technology, Wuhan 430014, China*

Dan Jin − *School of Laboratory Medicine, Hubei University of Chinese Medicine, Wuhan 430065, China*

Complete contact information is available at: https://pubs.acs.org/10.1021/acssensors.0c00772

Notes

The authors declare no competing financial interest.

ACKNOWLEDGMENTS

This work was supported by the National Natural Science Foundation of China (21775034, 21974037 and 21974035), Science Foundation for Distinguished Young Scholars of Hubei Province (2018CFA041), and Guangxi Medical University Training program for Distinguished Young Scholars.

REFERENCES

(1) Ji, C.; Guo, X. The clinical potential of circulating microRNAs in obesity. *Nat. Rev. Endocrinol.* **2019**, *15*, 731−743.

(2) Mitchell, P. S.; Parkin, R. K.; Kroh, E. M.; Fritz, B. R.; Wyman, S. K.; Pogosova-Agadjanyan, E. L.; Peterson, A.; Noteboom, J.; O'Briant, K. C.; Allen, A.; Lin, D. W.; Urban, N.; Drescher, C. W.; Knudsen, B. S.; Stirewalt, D. L.; Gentleman, R.; Vessella, R. L.; Nelson, P. S.; Martin, D. B.; Tewari, M. Circulating microRNAs as stable blood-based markers for cancer detection. *Proc. Natl. Acad. Sci. U. S. A.* **2008**, *105*, 10513−10518.

(3) Dave, V. P.; Ngo, T. A.; Pernestig, A.-K.; Tilevik, D.; Kant, K.; Nguyen, T.; Wolff, A.; Bang, D. D. MicroRNA amplification and detection technologies: opportunities and challenges for point of care diagnostics. *Lab. Invest.* **2019**, *99*, 452−469.

(4) Dong, H.; Lei, J.; Ding, L.; Wen, Y.; Ju, H.; Zhang, X. MicroRNA: Function, Detection, and Bioanalysis. *Chem. Rev.* **2013**, *113*, 6207−6233.

(5) Wanunu, M.; Dadosh, T.; Ray, V.; Jin, J.; McReynolds, L.; Drndić, M. Rapid electronic detection of probe-specific microRNAs using thin nanopore sensors. *Nat. Nanotechnol.* **2010**, *5*, 807−814.

(6) Duan, D.; Zheng, K.-x.; Shen, Y.; Cao, R.; Jiang, L.; Lu, Z.; Yan, X.; Li, J. Label-free high-throughput microRNA expression profiling from total RNA. *Nucleic Acids Res.* **2011**, *39*, No. e154.

(7) Ren, Y.; Deng, H.; Shen, W.; Gao, Z. A Highly Sensitive and Selective Electrochemical Biosensor for Direct Detection of MicroRNAs in Serum. *Anal. Chem.* **2013**, *85*, 4784−4789.

(8) Shi, K.; Dou, B.; Yang, C.; Chai, Y.; Yuan, R.; Xiang, Y. DNA-Fueled Molecular Machine Enables Enzyme-Free Target Recycling Amplification for Electronic Detection of MicroRNA from Cancer Cells with Highly Minimized Background Noise. *Anal. Chem.* **2015**, *87*, 8578−8583.

(9) Wen, Y.; Li, L.; Li, J.; Lin, M.; Liu, G.; Liang, W.; Xu, L.; Li, Y.; Zuo, X.; Ren, S.; Zhu, Y. DNA Framework-Mediated Electrochemical Biosensing Platform for Amplification-Free MicroRNA Analysis. *Anal. Chem.* **2020**, *92*, 4498−4503.

(10) Ge, Z.; Lin, M.; Wang, P.; Pei, H.; Yan, J.; Shi, J.; Huang, Q.; He, D.; Fan, C.; Zuo, X. Hybridization Chain Reaction Amplification of MicroRNA Detection with a Tetrahedral DNA Nanostructure-Based Electrochemical Biosensor. *Anal. Chem.* **2014**, *86*, 2124−2130.

(11) Feng, C.; Mao, X.; Shi, H.; Bo, B.; Chen, X.; Chen, T.; Zhu, X.; Li, G. Detection of microRNA: A Point-of-Care Testing Method Based on a pH-Responsive and Highly Efficient Isothermal Amplification. *Anal. Chem.* **2017**, *89*, 6631−6636.

(12) Gai, P.; Gu, C.; Li, H.; Sun, X.; Li, F. Ultrasensitive Ratiometric Homogeneous Electrochemical MicroRNA Biosensing via Target-Triggered Ru(III) Release and Redox Recycling. *Anal. Chem.* **2017**, *89*, 12293−12298.

(13) Qiu, X.; Zhang, H.; Yu, H.; Jiang, T.; Luo, Y. Duplex-specific nuclease-mediated bioanalysis. *Trends Biotechnol.* **2015**, *33*, 180−188.

(14) Wu, Y.; Tilley, R. D.; Gooding, J. J. Challenges and Solutions in Developing Ultrasensitive Biosensors. *J. Am. Chem. Soc.* **2019**, *141*, 1162−1170.

(15) Hu, T.; Zhang, L.; Wen, W.; Zhang, X.; Wang, S. Enzyme catalytic amplification of miRNA-155 detection with graphene quantum dot-based electrochemical biosensor. *Biosens. Bioelectron.* **2016**, *77*, 451−456.

(16) Shen, J.; Li, Y.; Gu, H.; Xia, F.; Zuo, X. Recent Development of Sandwich Assay Based on the Nanobiotechnologies for Proteins, Nucleic Acids, Small Molecules, and Ions. *Chem. Rev.* **2014**, *114*, 7631−7677.

(17) Lee, J. U.; Kim, W. H.; Lee, H. S.; Park, K. H.; Sim, S. J. Quantitative and Specific Detection of Exosomal miRNAs for Accurate Diagnosis of Breast Cancer Using a Surface-Enhanced Raman Scattering Sensor Based on Plasmonic Head-Flocked Gold Nanopillars. *Small* **2019**, *15*, 1804968.

(18) Liu, L.; Lu, H.; Shi, R.; Peng, X.-X.; Xiang, Q.; Wang, B.; Wan, Q.-Q.; Sun, Y.; Yang, F.; Zhang, G.-J. Synergy of Peptide−Nucleic Acid and Spherical Nucleic Acid Enabled Quantitative and Specific Detection of Tumor Exosomal MicroRNA. *Anal. Chem.* **2019**, *91*, 13198−13205.

(19) Arata, H.; Komatsu, H.; Han, A.; Hosokawa, K.; Maeda, M. Rapid microRNA detection using power-free microfluidic chip: coaxial stacking effect enhances the sandwich hybridization. *Analyst* **2012**, *137*, 3234−3237.

(20) Clancy, E.; Burke, M.; Arabkari, V.; Barry, T.; Kelly, H.; Dwyer, R. M.; Kerin, M. J.; Smith, T. J. Amplification-free detection of microRNAs via a rapid microarray-based sandwich assay. *Anal. Bioanal. Chem.* **2017**, *409*, 3497−3505.

(21) Shi, R.; Hu, Z.; Lu, H.; Liu, L.; Xu, L.; Liu, Y.; Wu, H.; Huang, B.; Zhang, G.-J.; Chen, S.; Yang, F. Hierarchical Nanostructuring Array Enhances Mid-Hybridization for Accurate Herbal Identification via ITS2 DNA Barcode. *Anal. Chem.* **2020**, *92*, 2136−2144.

(22) Ye, L.; Yang, F.; Ding, Y.; Yu, H.; Yuan, L.; Dai, Q.; Sun, Y.; Wu, X.; Xiang, Y.; Zhang, G.-J. Bioinspired Trans-Scale Functional Interface for Enhanced Enzymatic Dynamics and Ultrasensitive Detection of microRNA. *Adv. Funct. Mater.* **2018**, *28*, 1706981.

(23) De Luna, P.; Mahshid, S. S.; Das, J.; Luan, B.; Sargent, E. H.; Kelley, S. O.; Zhou, R. High-Curvature Nanostructuring Enhances Probe Display for Biomolecular Detection. *Nano Lett.* **2017**, *17*, 1289−1295.
(24) Sage, A. T.; Besant, J. D.; Lam, B.; Sargent, E. H.; Kelley, S. O. Ultrasensitive Electrochemical Biomolecular Detection Using Nanostructured Microelectrodes. *Acc. Chem. Res.* **2014**, *47*, 2417−2425.
(25) Soleymani, L.; Fang, Z.; Sargent, E. H.; Kelley, S. O. Programming the detection limits of biosensors through controlled nanostructuring. *Nat. Nanotechnol.* **2009**, *4*, 844−848.
(26) Yang, H.; Hui, A.; Pampalakis, G.; Soleymani, L.; Liu, F.-F.; Sargent, E. H.; Kelley, S. O. Direct, Electronic MicroRNA Detection for the Rapid Determination of Differential Expression Profiles. *Angew. Chem., Int. Ed.* **2009**, *48*, 8461−8464.
(27) Li, Y.; Li, W.; Ouyang, Q.; Hu, S.; Tang, J. Detection of lung cancer with blood microRNA-21 expression levels in Chinese population. *Oncol. Lett.* **2011**, *2*, 991−994.
(28) Zhang, J.; Song, S.; Wang, L.; Pan, D.; Fan, C. A gold nanoparticle-based chronocoulometric DNA sensor for amplified detection of DNA. *Nat. Protoc.* **2007**, *2*, 2888−2895.
(29) Wang, S.; Yang, F.; Jin, D.; Dai, Q.; Tu, J.; Liu, Y.; Ning, Y.; Zhang, G.-J. Toehold Mediated One-Step Conformation-Switchable "Signal-On" Electrochemical DNA Sensing Enhanced with Homogeneous Enzymatic Amplification. *Anal. Chem.* **2017**, *89*, 5349−5356.
(30) Yakovchuk, P.; Protozanova, E.; Frank-Kamenetskii, M. D. Base-stacking and base-pairing contributions into thermal stability of the DNA double helix. *Nucleic Acids Res.* **2006**, *34*, 564−574.
(31) Lu, W.; Chen, Y.; Liu, Z.; Tang, W.; Feng, Q.; Sun, J.; Jiang, X. Quantitative Detection of MicroRNA in One Step via Next Generation Magnetic Relaxation Switch Sensing. *ACS Nano* **2016**, *10*, 6685−6692.
(32) Gao, Y.; Qiang, L.; Chu, Y.; Han, Y.; Zhang, Y.; Han, L. Microfluidic chip for multiple detection of miRNA biomarkers in breast cancer based on three-segment hybridization. *AIP Adv.* **2020**, *10*, 045022.
(33) Steel, A. B.; Herne, T. M.; Tarlov, M. J. Electrochemical Quantitation of DNA Immobilized on Gold. *Anal. Chem.* **1998**, *70*, 4670−4677.
(34) Deng, M.; Li, M.; Li, F.; Mao, X.; Li, Q.; Shen, J.; Fan, C.; Zuo, X. Programming Accessibility of DNA Monolayers for Degradation-Free Whole-Blood Biosensors. *ACS Mater. Lett.* **2019**, *1*, 671−676.
(35) Su, S.; Wu, Y.; Zhu, D.; Chao, J.; Liu, X.; Wan, Y.; Su, Y.; Zuo, X.; Fan, C.; Wang, L. On-Electrode Synthesis of Shape-Controlled Hierarchical Flower-Like Gold Nanostructures for Efficient Interfacial DNA Assembly and Sensitive Electrochemical Sensing of MicroRNA. *Small* **2016**, *12*, 3794−3801.
(36) Ma, D.; Huang, C.; Zheng, J.; Tang, J.; Li, J.; Yang, J.; Yang, R. Quantitative detection of exosomal microRNA extracted from human blood based on surface-enhanced Raman scattering. *Biosens. Bioelectron.* **2018**, *101*, 167−173.
(37) Li, B.; Ren, S.; Li, X.; Wang, Y.; Garfield, D.; Zhou, S.; Chen, X.; Su, C.; Chen, M.; Kuang, P.; Gao, G.; He, Y.; Fan, L.; Fei, K.; Zhou, C.; Schmit-Bindert, G. MiR-21 overexpression is associated with acquired resistance of EGFR-TKI in non-small cell lung cancer. *Lung Canc.* **2014**, *83*, 146−153.
(38) Yan, L.-X.; Huang, X.-F.; Shao, Q.; Huang, M.-Y.; Deng, L.; Wu, Q.-L.; Zeng, Y.-X.; Shao, J.-Y. MicroRNA miR-21 overexpression in human breast cancer is associated with advanced clinical stage, lymph node metastasis and patient poor prognosis. *RNA* **2008**, *14*, 2348−2360.
(39) Feng, Y.-H.; Tsao, C.-J. Emerging role of microRNA-21 in cancer. *Biomed. Rep.* **2016**, *5*, 395−402.
(40) Tian, L.; Shan, W.; Zhang, Y.; Lv, X.; Li, X.; Wei, C. Up-Regulation of miR-21 Expression Predicate Advanced Clinicopathological Features and Poor Prognosis in Patients with Non-Small Cell Lung Cancer. *Pathol. Oncol. Res.* **2016**, *22*, 161−167.
(41) Venturutti, L.; Romero, L. V.; Urtreger, A. J.; Chervo, M. F.; Cordo Russo, R. I.; Mercogliano, M. F.; Inurrigarro, G.; Pereyra, M. G.; Proietti, C. J.; Izzo, F.; Díaz Flaqué, M. C.; Sundblad, V.; Roa, J. C.; Guzmán, P.; Bal de Kier Joffé, E. D.; Charreau, E. H.; Schillaci, R.; Elizalde, P. V. Stat3 regulates ErbB-2 expression and co-opts ErbB-2 nuclear function to induce miR-21 expression, PDCD4 down-regulation and breast cancer metastasis. *Oncogene* **2016**, *35*, 2208−2222.
(42) Jalali, M.; AbdelFatah, T.; Mahshid, S. S.; Labib, M.; Sudalaiyadum Perumal, A.; Mahshid, S. A Hierarchical 3D Nanostructured Microfluidic Device for Sensitive Detection of Pathogenic Bacteria. *Small* **2018**, *14*, 1801893.
(43) Yang, F.; Li, Q.; Wang, L.; Zhang, G.-J.; Fan, C. Framework-Nucleic-Acid-Enabled Biosensor Development. *ACS Sens.* **2018**, *3*, 903−919.
(44) Ge, Z.; Gu, H.; Li, Q.; Fan, C. Concept and Development of Framework Nucleic Acids. *J. Am. Chem. Soc.* **2018**, *140*, 17808−17819.
(45) Smith, S. J.; Nemr, C. R.; Kelley, S. O. Chemistry-Driven Approaches for Ultrasensitive Nucleic Acid Detection. *J. Am. Chem. Soc.* **2017**, *139*, 1020−1028.
(46) Tavallaie, R.; McCarroll, J.; Le Grand, M.; Ariotti, N.; Schuhmann, W.; Bakker, E.; Tilley, R. D.; Hibbert, D. B.; Kavallaris, M.; Gooding, J. J. Nucleic acid hybridization on an electrically reconfigurable network of gold-coated magnetic nanoparticles enables microRNA detection in blood. *Nat. Nanotechnol.* **2018**, *13*, 1066−1071.
(47) Yasui, T.; Yanagida, T.; Ito, S.; Konakade, Y.; Takeshita, D.; Naganawa, T.; Nagashima, K.; Shimada, T.; Kaji, N.; Nakamura, Y.; Thiodorus, I. A.; He, Y.; Rahong, S.; Kanai, M.; Yukawa, H.; Ochiya, T.; Kawai, T.; Baba, Y. Unveiling massive numbers of cancer-related urinary-microRNA candidates via nanowires. *Sci. Adv.* **2017**, *3*, No. e1701133.

https://dx.doi.org/10.1021/acssensors.0c00772
ACS Sens. 2020, 5, 2514−2522